I&EC research
Industrial & Engineering Chemistry Research

Article

Cite This: Ind. Eng. Chem. Res. 2018, 57, 16657−16663

pubs.acs.org/IECR

Understanding Alkane Dehydrogenation through Alcohol Dehydration on γ-Al_2O_3

Pavlo Kostetskyy, Carly M. Nolan, Mudit Dixit, and Giannis Mpourmpakis*

Department of Chemical Engineering, University of Pittsburgh, Pittsburgh, Pennsylvania 15261, United States

Supporting Information

ABSTRACT: Nonoxidative dehydrogenation of alkanes is an important chemical reaction, as it can be used for production of olefins, commonly used as building blocks for a range of plastics and chemicals. Several metal oxides, including γ-Al_2O_3, have exhibited dehydrogenation activity, showing promise as candidates for the upgrade of alkanes. In this work we use computational chemistry methods to investigate the mechanism of ethane, propane, *n*-butane, and *i*-butane dehydrogenation pathways on strong Lewis acid−base sites of γ-Al_2O_3. On the basis of our calculations, it was shown that a concerted dehydrogenation mechanism is energetically preferred with the formation of a carbenium-ion-like transition state. An alkane dehydrogenation model was developed on the basis of methodology previously applied in structure−activity relations (SAR) for alcohol dehydration on metal oxides. The carbenium ion stability (CIS), shown to be a descriptor in alcohol dehydration, was used as a quantitative descriptor in alkane dehydrogenation and was found to correlate with the calculated activation energy barriers for the hydrocarbons in question. Increased hydrocarbon substitution (branching) was found to decrease the calculated reaction barriers, on the basis of the CIS at the transition state. Importantly, SARs developed for alcohol dehydration on various metal oxides were found to accurately capture the catalytic activity trends in alkane dehydrogenation, accounting for catalyst acid−base surface properties and the CIS of intermediates at the transition state. These results highlight that identifying the appropriate physicochemical descriptors of catalysts can accurately describe a different set of reactions (alcohol dehydration vs alkane dehydrogenation) as long as these reactions progress with similar transition states. Such models can accelerate the discovery of highly active metal oxide catalysts for the production of olefins.

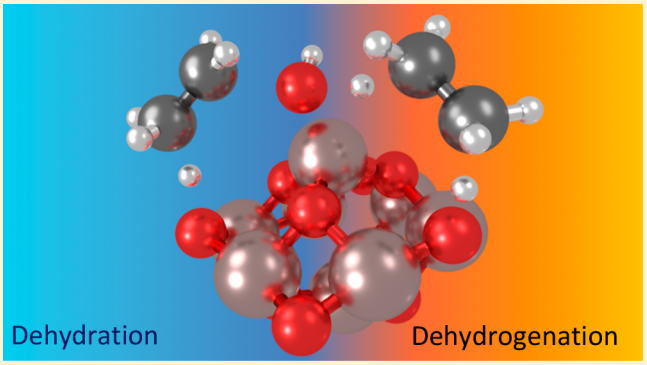

INTRODUCTION

Olefins are important chemical building blocks for the production of a wide range of valuable chemicals and plastics, with increasing demand worldwide.[1−3] The low cost and high abundance of alkanes has motivated significant work in the field of olefin production via catalytic dehydrogenation. A number of catalysts have been evaluated for selective dehydrogenation of alkanes to form alkenes through both oxidative and nonoxidative dehydrogenation reactions. Metal oxides exhibiting acid−base surface functionalities have shown promise as nonoxidative dehydrogenation catalysts. Several oxide materials were shown to exhibit moderate to high catalytic activity, including Al_2O_3, Ga_2O_3, Cr_2O_3, and others.[1−8] Nakagawa et al. have shown that supported and unsupported Ga_2O_3 was active in oxidative alkane dehydrogenation, along with Cr_2O_3, Fe_2O_3, Al_2O_3, and SiO_2.[6] Although Ga_2O_3 has shown good dehydrogenation activity, a significant issue that remains is catalyst deactivation. To combat catalyst deactivation, stable supports can be used to increase the stability of the metal oxide.[2]

Group 5 and 6 transition metal oxides, typically supported on a stable oxide support, have also shown promise as highly active, selective, and robust alkane dehydrogenation catalysts, finding wide industrial application.[2,3,5−7,9−14] These catalyst systems are characterized by the presence of isolated surface sites that are active in catalyzing the dehydrogenation of alkanes. The CATOFIN process is based on chromium oxide catalyst supported on alumina[11] and is industrially used to produce propylene and isobutene from their corresponding alkanes. The complexity of the system has led to debate concerning the nature of surface active sites, with recent work pointing to isolated Cr^{3+} surface species or small chromium oxide clusters, as the likely active sites.[15−17]

Alkane dehydrogenation mechanisms on metal oxide active sites are debated in literature studies and vary with the type of catalysts and the nature of active sites present.[18−20] Metal−alkyl complexes have been shown to be intermediates in alkane dehydrogenation on several oxides;[8,15−17] however, it is not clear if these species are reaction intermediates or spectators in

Received: September 8, 2018
Revised: November 2, 2018
Accepted: November 12, 2018
Published: November 12, 2018

DOI: 10.1021/acs.iecr.8b04392
Ind. Eng. Chem. Res. 2018, 57, 16657−16663

the production of olefins.[15−17] Activation takes place on metal (Lewis acid) centers on the oxide surface, forming organometallic intermediates (M−alkyl), which proceed to hydrogen elimination and olefin formation. Isolated metal centers of low coordination exhibit high activity.[8] Aluminum oxide is known to exhibit strong acid−base properties,[21] with recent work by Hargreaves et al.[4] showing Al_2O_3 to be active in H/D exchange reactions. The authors attributed the increased activity to inherent Lewis acidity and basicity of surface acid−base pairs, exhibiting the highest quantities for undercoordinated surface sites.

Recent experimental work on alkane dehydrogenation by Rodemerck et al.[22] has shown aluminum oxide to be an active catalyst in nonoxidative dehydrogenation of propane, exhibiting good activity and selectivity toward the olefin product. The authors attributed the observed catalytic activity to the presence of coordinatively unsaturated Lewis acid−base sites, generated at high temperatures by removal of surface hydroxyl groups which form in the presence of water.[23,24] Surface hydroxylation can poison the catalyst surface and is a commonly observed phenomenon, studied extensively in recent experimental and computational studies.[23,24] High-temperature pretreatment of the catalyst or extended time on stream under the reaction conditions likely removes surface water, thus exposing the most active surface sites.[23−25] Joubert et al. investigated propane dehydrogenation activity of Al_2O_3 support and showed that dehydrogenation can occur with moderate activation barriers.[26,27] The authors evaluated nonoxidative propane dehydrogenation via concerted and sequential pathways, with the former proceeding via dissociation of two C−H bonds in a single catalytic step.

Of the different thermodynamic phases of alumina, γ-Al_2O_3 has been shown to be an active catalyst and a stable support material for a range of catalytic applications and various chemistries.[4,20,25,28−31] The exact crystallographic structure of bulk alumina is not well-defined, but it is known that Al^{3+} cations are distributed within the bulk in tetrahedral and octahedral positions, exposing undercoordinated surface sites of Al−O Lewis acid−base pairs.[23,24] Tricoordinated aluminum centers (Al^{CN3}) have been shown to exist on the (110) facets of γ-Al_2O_3[23−25,31] and were reported to exhibit the highest degree of Lewis acidity.[31] Cluster models of strongly acidic tricoordinated Al^{3+} Lewis acid sites on γ-Al_2O_3 have been used as representative of the local coordination environment on alumina (110) facets. These models were used in several recent computational studies of alcohol dehydration chemistry.[28,30,32] Excellent agreement was observed between calculated activation energy barriers and those measured experimentally for alcohols of varying chain length and degree of substitution.[28] In addition, alcohol dehydration structure−activity relationships (SAR) were constructed on the basis of physicochemical descriptors of the catalyst and reacting alcohols that can aid in screening the reactivity of different oxides/reactants.[29,30]

Progress has been made in understanding the surface chemistry on oxides in terms of active sites and mechanisms; however, debate still exists in both areas, and significant research is still required. Further research on alkane dehydrogenation on γ-Al_2O_3 can provide a more complete mechanistic understanding, adding to the current state of the art. Toward this goal, in our most recent work, we investigated the propane nonoxidative dehydrogenation on different surface sites of γ-Al_2O_3 and revealed that the dissociative H_2 adsorption can be a descriptor for Lewis acid−base strength.[33] In addition, the effect of surface hydroxylation on catalytic performance was evaluated explicitly and shown that under dehydrogenation conditions tricoordinated Al sites can survive on metastable γ-Al_2O_3 surfaces (generated through high-temperature pretreatment) that can be catalytically active.[33] In this work we investigate the nonoxidative dehydrogenation of several alkanes of varying size and degree of branching (ethane, propane, *n*-butane, and *i*-butane) over an alumina cluster model of γ-Al_2O_3, which exposes undercoordinated Al^{3+} acid centers using *ab initio* electronic structure calculations. We examine two competing mechanisms on acid−base site pairs of the oxide surface, namely, a sequential and a concerted pathway for the four hydrocarbons in question and show an energetic preference for the concerted pathway in all cases. Finally, using a previously reported alcohol dehydration model,[30] we developed an alkane dehydrogenation model, based on fundamental properties of the catalyst and reacting hydrocarbons, as a potential reactivity screening tool. This work demonstrates that different reactions (alcohol dehydration vs alkane dehydrogenation) that evolve through similar mechanisms (i.e., concerted elimination) can be described using the same catalyst (Lewis acid/base functionalities) and reactant (carbenium ion stability) properties. The development of such models can aid in accelerating metal oxide catalyst discovery.

COMPUTATIONAL METHODS

DFT calculations were performed to study alumina-catalyzed dehydrogenation of ethane, propane, *n*-butane, and *i*-butane. Cluster models have been used extensively as model systems to investigate species adsorption and reactions on metal oxide surfaces and shown to accurately capture the physics of surface reactions.[28,34] The model cluster used in this work (Figure 1, *vide infra*) consists of 8 metal and 12 oxygen atoms and has been previously used to simulate alcohol dehydration active sites (tricoordinated Lewis sites) on alumina, in excellent agreement with experimental dehydration results.[28] All energy calculations were performed using the B3LYP[35,36] hybrid functional as implemented in the Gaussian 09 package,[37] with

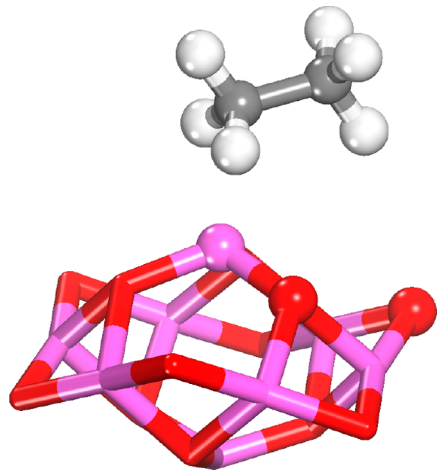

Figure 1. Ethane adsorption ground state on the Al^{CN3} site of the Al_8O_{12} cluster. Aluminum atoms are shown in magenta, oxygen in red, carbon in gray, and hydrogen in white. For visual clarity, hydrocarbon and Al_2O_3 cluster atoms (site pairs) that participate in the chemistry are represented as spheres.

DOI: 10.1021/acs.iecr.8b04392
Ind. Eng. Chem. Res. 2018, 57, 16657−16663

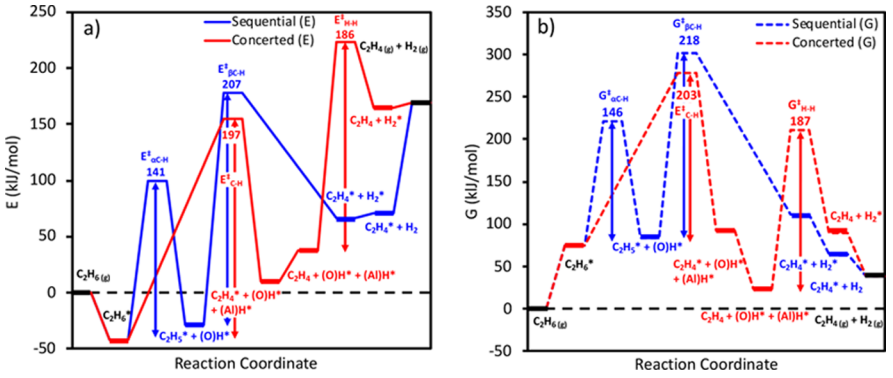

Figure 2. Reaction energy profiles of ethane dehydrogenation via the concerted (red) and sequential (blue) pathways in terms of (a) electronic energies, *E*, and (b) Gibbs free energies, *G*. Energies of ground states and saddle points were referenced to reactants at infinite separation. Reaction barrier values for corresponding reaction steps are reported on the energy diagram. Values are reported in kJ/mol; adsorbed states are denoted with asterisks (*), and transition states are denoted with double daggers (‡).

the 6-311G* triple-ζ basis set. Reaction pathways were mapped by scanning the potential energy surface of the reaction coordinate. The energy maxima were fully relaxed to a saddle point to locate the actual transition states. In addition, we used the synchronous transit-guided quasi-Newton (STQN) method to locate relevant transition states. All transition states and local minima were obtained by full optimizations and verified by vibrational frequency and intrinsic reaction coordinate (IRC) calculations.[38] Natural bond orbital (NBO) charge analysis was applied to calculate the partial charges reported in this work (*vide infra*). The binding energy (BE) of reactants on the Lewis acid site of the metal oxide clusters was calculated according to eq 1:

$$\mathrm{BE} = E_{\mathrm{ads}} - E_{\mathrm{cluster}} - E_{\mathrm{react}} \quad (1)$$

Here, E_{ads} is the total electronic energy of an adsorbed alkane on the oxide cluster, and E_{cluster} and E_{react} are the total electronic energies of the bare cluster and alkanes, respectively. Proton affinity (PA) was used to quantify strength of oxygen base sites and was calculated according to eq 2.

$$\mathrm{PA} = E_{\mathrm{cluster+H^+}} - E_{\mathrm{cluster}} \quad (2)$$

Here, $E_{\mathrm{cluster+H}}{}^{+}$ and E_{cluster} are the energies of the protonated and bare (neutral) cluster, as the electronic energy of a proton is zero.

RESULTS AND DISCUSSION

Although theoretical and experimental studies have been performed to elucidate the reaction mechanism for non-oxidative alkane dehydrogenation,[1] extensive debate remains regarding the surface mechanism. We begin by assessing dehydrogenation of ethane via two different mechanisms, a sequential and a concerted pathway on surface Lewis acid–base site pairs of the Al_8O_{12} cluster model shown in Figure 1.

Reaction energetics of the two mechanisms are reported in Figure 2, in terms of the electronic (*E*) and Gibbs (*G*) free energies. The free energies were calculated at a temperature of 823 K, typical of experimental dehydrogenation operating conditions. The first step in both mechanisms is adsorption of hydrocarbons on the active site of the catalyst that is weakly exothermic in terms of electronic energies and endergonic in terms of Gibbs free energies. The weak adsorption is characteristic of the high chemical stability of (saturated) alkanes that makes them difficult to process in catalytic applications. Detailed energetics of alkane adsorption on the active site can be found in Table S3 of the Supporting Information.

From the adsorbed state (C_2H_6*), the sequential mechanism (blue lines in Figure 2) is initiated by activation of a C–H bond (αC–H) and formation of an Al-bound organometallic complex with a neighboring O–H group (C_2H_5* + (O)H*) via heterolytic splitting. A number of alternative ground states were considered, including an alkoxide-like (O)C_2H_5* species bound on a neighboring oxygen base site; however, the Al-bound C_2H_5 was found to be the most stable adsorption configuration. For the sequential pathway, the barrier for the initial C–H activation was found to be moderate, with calculated values of 141 and 146 kJ/mol in terms of electronic (*E*) and free (*G*) energies, respectively. The next step in the sequential route was found to be the direct formation of molecular H_2 by elimination of the β-hydrogen, featuring a 6-membered transition state (Figure 3a). The

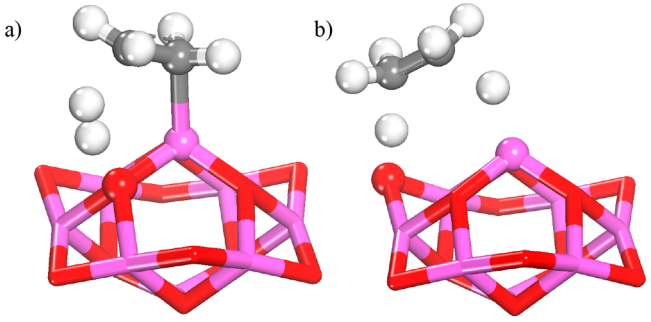

Figure 3. Graphical representation of transition states in β-hydrogen elimination to form molecular H_2 in the sequential pathway (a) and concerted hydrogen elimination to form ethylene and (dissociated) surface-bound hydrogen (b). For visual clarity, hydrocarbon and Al_2O_3 cluster atoms (site pairs) that participate in the chemistry are represented as spheres.

activation barrier ($E^{\ddagger}_{\beta\mathrm{C-H}}$) for this step was shown to be rate-limiting, with calculated values of 207 and 218 kJ/mol, in terms of electronic and free energies, respectively. The catalytic cycle is completed by desorption of the weakly bound H_2 and ethylene adsorbates to regenerate the catalyst surface, with a net reaction endothermicity of 170 and 39 kJ/mol in terms of electronic and free energies, respectively.

In the concerted pathway (red lines in Figure 2), upon adsorption, the alkane molecule proceeds to dehydrogenate

DOI: 10.1021/acs.iecr.8b04392
Ind. Eng. Chem. Res. 2018, 57, 16657–16663

directly to the olefin product via simultaneous cleavage of two C−H bonds. The activation energy barriers ($E^{\ddagger}_{C-H}$) were found to be lower than those in the sequential pathway, with calculated electronic and free energy values of 197 and 203 kJ/mol, respectively. The concerted pathway features a 6-center transition state (Figure 3b) in which the surface Lewis acid center and a neighboring base site abstract the hydrogen atoms, resulting in formation of the alkene and a surface-bound hydrogen in the dissociated state. The catalytic cycle is completed by formation of molecular hydrogen via an associative transition state between the Al^{CN3} and a peripheral oxygen base site, with calculated electronic and free energy barriers of 186 and 187 kJ/mol, respectively (Figure 2). It is important to note that this hydrogen formation barrier is quite high between the 2-fold coordinated peripheral oxygen site and the acid center; however, it is plausible that a surface oxygen-bound proton can diffuse on the oxide surface to a 3-fold coordinated base site that is in closer proximity to the Al^{CN3} center. The surface diffusion barrier was calculated to be 119 kJ/mol in terms of electronic energy. The corresponding hydrogen formation barriers between the neighboring acid−base pair decrease to 135 and 136 kJ/mol in terms of electronic and free energy barriers, respectively.

On the basis of the potential energy landscape shown in Figure 2, the rate-limiting elementary steps in the concerted pathway are favored relative to the sequential route by 15 kJ/mol in Gibbs free energy. The free energies reported in Figure 2 appear to reveal an entropic effect (at elevated dehydrogenation temperatures) that further favors the concerted pathway, as evidenced by the exergonic (favored) desorption of alkene and H_2 products and comparable free energy barriers for all elementary steps. This energetic preference of the concerted pathway was confirmed for all the hydrocarbons considered in this work, with the calculated reaction barriers reported in Table 1. In addition, the relevant barriers for the sequential pathway are reported in Table 2, showing barriers for the initial C−H activation (TS1) and the subsequent β-hydrogen elimination (TS2), in terms of electronic and free energy barriers, respectively. A comparison of activation energies, enthalpies, and entropies at the transition states of rate-limiting elementary steps for the concerted and sequential pathways in the dehydrogenation of ethane is reported in Table S4 of the Supporting Information. As can be seen, the free energy difference between the two pathways is enthalpically driven, with a negligible difference in entropic losses observed at the transition state. Additionally, the energetic span approximation of Kozuch et al.[39] was applied to the dehydrogenation reaction energetics for the four hydrocarbons in question. We calculated turnover frequency (TOF) values for the four hydrocarbons in question, on the basis of the electronic and free energy profiles along the reaction coordinate (Table S5). The calculated TOF values favor the sequential pathway in terms of electronic energies. This trend is reversed when accounting for the free energies, favoring the concerted pathway for all hydrocarbons in question. This also confirms the requirement of energy input (i.e., elevated temperature) to drive this chemistry since the TOFs of the concerted, free energy pathway increase when accounting for temperature effects, whereas they become negligibly small for the sequential, electronic energy pathway.

It should be noted that the barriers reported in Table 1 correspond to reactions involving the more basic 2-fold coordinated oxygen site on the periphery of the cluster (see Figure 1). However, concerted dehydrogenation barriers corresponding to reactions between the neighboring 3-fold-coordinated oxygen center and Al^{CN3} are increased (see Figure 4), due to the decreased basicity of the more coordinated O^{CN3} (compared to O^{CN2}). Finally, it should be noted that the transition state for isobutane dehydrogenation via the concerted pathway could not be located in the case involving the O^{CN3} site, after exhausting a number of available computational methods and transition state searches. This can be potentially rationalized by the bulky nature of the molecule and short interatomic distance of the Al^{CN3}−O^{CN3} site pair. The calculated dehydrogenation reaction energetics for all four hydrocarbons via the sequential and concerted pathways are reported in Figures S1−S4 of the Supporting Information (SI) document.

A clear effect of alkane substitution can be observed in terms of calculated barriers for the concerted pathway, with the barriers decreasing for more substituted species. The transition state in the concerted elimination pathway was found to have

Table 1. Calculated C−H Activation Barriers for the Concerted Pathway in Terms of Electronic (E) and Free (G) Energies, Reported in kJ/mol

species	E_a (kJ/mol)	G_a (kJ/mol)
ethane	197	203
propane	169	170
n-butane	169	168
i-butane	148	156

Table 2. Calculated Elementary Activation Barriers for the Sequential Pathway in Terms of Electronic and Free Energies

species	TS1-E_a (kJ/mol)	TS1-G_a (kJ/mol)	TS2-E_a (kJ/mol)	TS2-G_a (kJ/mol)
ethane	141	146	207	218
propane	133	136	187	184
n-butane	136	132	184	186
i-butane	141	148	170	163

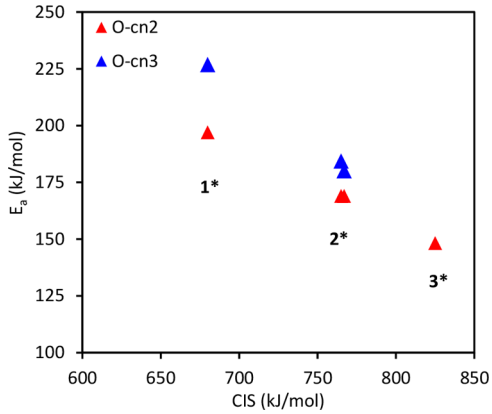

Figure 4. Calculated dehydrogenation (electronic) energy barriers for all alkanes involving the 2-fold-coordinated (red) and 3-fold-coordinated (blue) surface oxygen base sites plotted vs CIS. Data points corresponding to primary, secondary, and tertiary carbocation intermediates are denoted with numerical insets.

DOI: 10.1021/acs.iecr.8b04392
Ind. Eng. Chem. Res. 2018, 57, 16657−16663

carbenium ion character for all hydrocarbons, with calculated partial charges of +0.35, +0.61, +0.67, and +0.75 for ethane, propane, *n*-butane, and *i*-butane, respectively. The calculated partial charges are a function of the degree of (C−H) bond elongation toward the corresponding acid/base "acceptor" sites at the transition state, with the hydridic C−H bond being significantly more elongated relative to the protic. Furthermore, the difference in bond elongation increases for more substituted species, with the calculated distances reported in Table 3.

Table 3. Calculated C−H Bond Distances at the Transition State in the Concerted Pathway for the Four Hydrocarbons in Question[a]

species	C−H^{Al} (Å)	C−H^{OCN2} (Å)
ethane	1.612	1.416
propane	2.057	1.230
n-butane	2.143	1.204
i-butane	2.303	1.156

[a]Hydridic and protic hydrogens are denoted with Al and OCN2, respectively.

The increased partial charge (stability) of the more substituted species can be attributed to the presence of additional methyl (electron donating) substituents that stabilize the carbocation intermediate. The calculated partial charges in the transition state correlate with the calculated activation energies reported in Table 1 and are found to correlate linearly with carbenium ion stabilities (CIS) of the four hydrocarbons, as shown in Figure 4. CIS has been used as a physicochemical descriptor in alcohol dehydration chemistry which also involves formation of carbenium ions in the transition state.[29,30,40] CIS is defined as the proton binding energy of the alkene corresponding to the source alkane in the reaction, with larger values corresponding to higher stability of the more substituted species.[40]

In addition to a physicochemical descriptor for reactant stability (CIS), suitable descriptors can be used to quantify Lewis acidity and basicity of the catalyst surface. Reactant binding energy (BE) and base site proton affinity (PA) have been used as quantitative descriptors of surface acidity and basicity and applied in developing SARs for alcohol dehydration.[29,30] Using a methodology previously used in dehydration of alcohols on Lewis acid clusters,[29,30] we developed a dehydrogenation model (eq 3) that applies the aforementioned descriptors in alkane dehydrogenation, by performing a multiparameter linear regression of the calculated reaction barriers (see model details in the Supporting Information).

$$E_a = 620.3 - 0.39\text{CIS} - 0.59\text{BE} - 0.19\text{PA} \quad (3)$$

A comparison of model-predicted and DFT-calculated activation energies of the rate-limiting step for the concerted pathway is shown in Figure 5, with good agreement observed between the two sets. The effect of CIS and base site PA on the calculated reaction barriers is captured for all reactants, with the largest deviation observed for ethane activation energies.

Interestingly, SARs developed for alcohol dehydration reactions on model clusters of metal oxide catalysts[29,30] were able to capture the effect of reactant substitution (CIS) and catalyst acid−base properties (BE, PA) on model-predicted

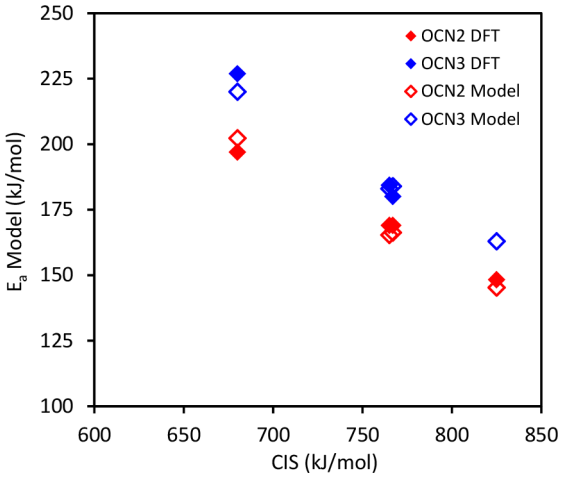

Figure 5. Calculated dehydrogenation energy barriers for all alkanes involving the 2-fold-coordinated (red) and 3-fold-coordinated (blue) surface oxygen base sites (◆) and the corresponding model predictions (◇). Values are reported in kJ/mol.

barrier values. This can be attributed to structural similarity at the transition state between alcohol dehydration and alkane dehydrogenation reactions, evolving through a concerted mechanism, shown in Figure S5 of the Supporting Information. A parity plot of DFT-calculated values versus SAR predictions of the dehydrogenation (red) and dehydration (blue) models is shown in Figure 6. The reaction barriers associated with

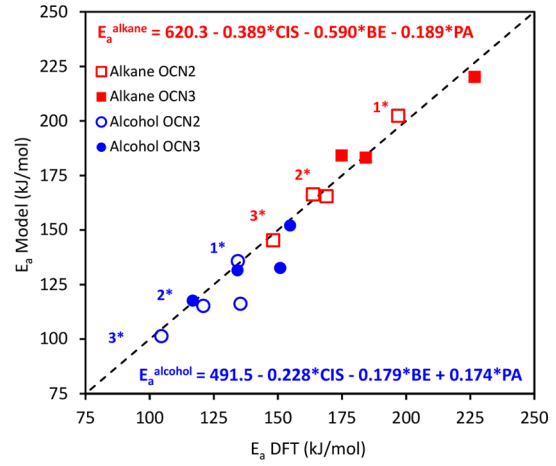

Figure 6. Parity plot of model-predicted and DFT-calculated reaction barriers for alkane dehydrogenation (red) and alcohol dehydration (blue). The calculated barriers are shown with respect to the coordination of the catalytic (oxygen) base site and substitution of hydrocarbons involved in the reactions (open and filled symbols). Model equations for the dehydrogenation and dehydration SARs are shown as figure insets. Values are reported in kJ/mol.

alcohol dehydration are well-captured by the previously developed[30] dehydration model, accounting for acid−base effects, and alcohol substitution. The fundamental difference between alcohol and alkane chemistry is captured by our descriptor-based models, where the strong binding of alcohols on Lewis acid sites of the oxides results in an anchoring effect, facilitating the dehydration to olefins. The high chemical stability of alkanes requires high energetic inputs (temperature) to catalyze their dehydrogenation, as reflected in experiments.[22,28,29]

DOI: 10.1021/acs.iecr.8b04392
Ind. Eng. Chem. Res. 2018, 57, 16657−16663

The dehydrogenation model developed in this work can be a useful screening tool in evaluating Lewis acid−base-catalyzed alkane systems for selective formation of olefins by non-oxidative dehydrogenation. The model accounts for fundamental system properties, quantified by descriptors of catalyst acidity (BE), basicity (PA), and reactant stability (CIS) in predicting the overall catalytic performance (activation energies). Importantly, the same fundamental descriptors also apply to alcohol dehydration chemistries on metal oxides. This highlights the flexibility of such a model as a tool in screening catalysts for different reactions based on the inherent physicochemical properties of the relevant active sites. Such models can aid the discovery of active and selective catalysts for the production of olefins and beyond.

CONCLUSIONS

Using *ab initio* electronic structure calculations, we studied the dehydrogenation of ethane, propane, *n*-butane, and *i*-butane over a strong Lewis acid site of a model catalyst system of γ-Al_2O_3. For this specific site, we propose the concerted dehydrogenation pathway to be energetically preferable, in terms of electronic and Gibbs free energies, to the sequential one, for all alkanes in question. A dependence on degree of reactant substitution and Lewis basicity was observed and quantified in terms of calculated activation energy barriers. Using physicochemical properties of this system we were able to develop SARs, designed as a screening tool to predict dehydrogenation performance for alkanes of varying size and substitution. These alkane dehydrogenation SARs have the same fundamental basis with alcohol dehydration SARs, due to the similarity of commonly observed concerted-elimination transition states in alkane dehydrogenation and alcohol dehydration. Importantly, this work highlights that SARs developed on metal oxides can be transferable to different reactions as long as the reaction mechanism is similar and the same catalyst properties govern catalytic reaction behavior.

ASSOCIATED CONTENT

Supporting Information

The Supporting Information is available free of charge on the ACS Publications website at DOI: 10.1021/acs.iecr.8b04392.

Energy profiles, graphical representations of transition states, and tables of parameter, energies, and turnover frequencies (PDF)

AUTHOR INFORMATION

Corresponding Author

*E-mail: gmpourmp@pitt.edu.

ORCID

Mudit Dixit: 0000-0001-9456-7806

Giannis Mpourmpakis: 0000-0002-3063-0607

Notes

The authors declare no competing financial interest.

ACKNOWLEDGMENTS

Acknowledgment is made to the Donors of the American Chemical Society Petroleum Research Fund (ACS-PRF, 56989-DNI5) for support of this research. The authors would also like to thank the Center for Research Computing (CRC) at the University of Pittsburgh for computational support.

REFERENCES

(1) Coperet, C. C-H Bond Activation and Organometallic Intermediates on Isolated Metal Centers on Oxide Surfaces. *Chem. Rev.* **2010**, *110* (2), 656−680.

(2) Banares, M. A. Supported metal oxide and other catalysts for ethane conversion: a review. *Catal. Today* **1999**, *51* (2), 319−348.

(3) McFarland, E. W.; Metiu, H. Catalysis by Doped Oxides. *Chem. Rev.* **2013**, *113* (6), 4391−4427.

(4) Hargreaves, J. S.J.; Hutchings, G. J.; Joyner, R. W.; Taylor, S. H. A study of the methane-deuterium exchange reaction over a range of metal oxides. *Appl. Catal., A* **2002**, *227* (1−2), 191−200.

(5) Michorczyk, P.; Ogonowski, J. Dehydrogenation of propane in the presence of carbon dioxide over oxide-based catalysts. *React. Kinet. Catal. Lett.* **2003**, *78* (1), 41−47.

(6) Nakagawa, K.; Okamura, M.; Ikenaga, N.; Suzuki, T.; Kobayashi, T.; et al. Dehydrogenation of ethane over gallium oxide in the presence of carbon dioxide. *Chem. Commun.* **1998**, No. 9, 1025−1026.

(7) Liu, Y.; Li, Z. H.; Lu, J.; Fan, K. N. Periodic Density Functional Theory Study of Propane Dehydrogenation over Perfect Ga2O3(100) Surface. *J. Phys. Chem. C* **2008**, *112* (51), 20382−20392.

(8) Kazansky, V. B.; Subbotina, I. R.; Pronin, A. A.; Schlogl, R.; Jentoft, F. C. Unusual infrared spectrum of ethane adsorbed by gallium oxide. *J. Phys. Chem. B* **2006**, *110* (15), 7975−7978.

(9) Blasco, T.; Nieto, J. M. L. Oxidative dehydrogenation of short chain alkanes on supported vanadium oxide catalysts. *Appl. Catal., A* **1997**, *157* (1−2), 117−142.

(10) Wachs, I. E.; Weckhuysen, B. M. Structure and reactivity of surface vanadium oxide species on oxide supports. *Appl. Catal., A* **1997**, *157* (1−2), 67−90.

(11) Weckhuysen, B. M.; Schoonheydt, R. A. Alkane dehydrogenation over supported chromium oxide catalysts. *Catal. Today* **1999**, *51* (2), 223−232.

(12) Nowak, I.; Ziolek, M. Niobium compounds: Preparation, characterization, and application in heterogeneous catalysis. *Chem. Rev.* **1999**, *99* (12), 3603−3624.

(13) Zheng, B.; Hua, W. M.; Yue, Y. H.; Gao, Z. Dehydrogenation of propane to propene over different polymorphs of gallium oxide. *J. Catal.* **2005**, *232* (1), 143−151.

(14) Otroshchenko, T.; Sokolov, S.; Stoyanova, M.; Kondratenko, V. A.; Rodemerck, U.; Linke, D.; Kondratenko, E. V. ZrO2-Based Alternatives to Conventional Propane Dehydrogenation Catalysts: Active Sites, Design, and Performance. *Angew. Chem., Int. Ed.* **2015**, *54* (52), 15880−15883.

(15) Lillehaug, S.; Borve, K. J.; Sierka, M.; Sauer, J. A. Catalytic dehydrogenation of ethane over mononuclear Cr(III) surface sites an silica. Part I. C-H activation by sigma-bond metathesis. *J. Phys. Org. Chem.* **2004**, *17* (11), 990−1006.

(16) Lillehaug, S.; Jensen, V. R.; Borve, K. J. Catalytic clehydrogenation of ethane over mononuclear Cr(III)-silica surface sites. Part 2: C-H activation by oxidative addition. *J. Phys. Org. Chem.* **2006**, *19* (1), 25−33.

(17) Olsbye, U.; Virnovskaia, A.; Prytz, O.; Tinnemans, S. J.; Weckhuysen, B. M. Mechanistic insight in the ethane dehydrogenation reaction over Cr/Al2O3 catalysts. *Catal. Lett.* **2005**, *103* (1−2), 143−148.

(18) Labinger, J. A.; Bercaw, J. E. Understanding and exploiting C-H bond activation. *Nature* **2002**, *417* (6888), 507−514.

(19) Baerns, M.; Buyevskaya, O. Simple chemical processes based on low molecular-mass alkanes as chemical feedstocks. *Catal. Today* **1998**, *45* (1−4), 13−22.

(20) Harlin, M. E.; Niemi, V. M.; Krause, A. O. I. Alumina-supported vanadium oxide in the dehydrogenation of butanes. *J. Catal.* **2000**, *195* (1), 67−78.

(21) Christiansen, M. A.; Mpourmpakis, G.; Vlachos, D. G. DFT-driven multi-site microkinetic modeling of ethanol conversion to ethylene and diethyl ether on gamma-Al2O3(111). *J. Catal.* **2015**, *323*, 121−131.

(22) Rodemerck, U.; Kondratenko, E. V.; Otroshchenko, T.; Linke, D. Unexpectedly high activity of bare alumina for non-oxidative

DOI: 10.1021/acs.iecr.8b04392
Ind. Eng. Chem. Res. 2018, 57, 16657−16663

isobutane dehydrogenation. *Chem. Commun.* **2016**, *52* (82), 12222−12225.
(23) Digne, M.; Sautet, P.; Raybaud, P.; Euzen, P.; Toulhoat, H. Hydroxyl groups on gamma-alumina surfaces: A DFT study. *J. Catal.* **2002**, *211* (1), 1−5.
(24) Digne, M.; Sautet, P.; Raybaud, P.; Euzen, P.; Toulhoat, H. Use of DFT to achieve a rational understanding of acid-basic properties of gamma-alumina surfaces. *J. Catal.* **2004**, *226* (1), 54−68.
(25) Valla, M.; Wischert, R.; Comas-Vives, A.; Conley, M. P.; Verel, R.; Coperet, C.; Sautet, P. Role of Tricoordinate Al Sites in CH3ReO3/Al2O3 Olefin Metathesis Catalysts. *J. Am. Chem. Soc.* **2016**, *138* (21), 6774−6785.
(26) Joubert, J.; Delbecq, F.; Thieuleux, C.; Taoufik, M.; Blanc, F.; Coperet, C.; Thivolle-Cazat, J.; Basset, J.-M.; Sautet, P. Synthesis, characterization, and catalytic properties of gamma-Al2O3-supported zirconium hydrides through a combined use of surface organometallic chemistry and periodic calculations. *Organometallics* **2007**, *26* (14), 3329−3335.
(27) Joubert, J.; Delbecq, F.; Sautet, P. Alkane metathesis by a tungsten carbyne complex grafted on gamma alumina: Is there a direct chemical role of the support? *J. Catal.* **2007**, *251* (2), 507−513.
(28) Roy, S.; Mpourmpakis, G.; Hong, D.-Y.; Vlachos, D. G.; Bhan, A.; Gorte, R. J. Mechanistic Study of Alcohol Dehydration on gamma-Al_2O_3. *ACS Catal.* **2012**, *2* (9), 1846−1853.
(29) Kostestkyy, P.; Yu, J.; Gorte, R. J.; Mpourmpakis, G. Structure-activity relationships on metal-oxides: alcohol dehydration. *Catal. Sci. Technol.* **2014**, *4* (11), 3861−3869.
(30) Kostetskyy, P.; Mpourmpakis, G. Structure-activity relationships in the production of olefins from alcohols and ethers: a first-principles theoretical study. *Catal. Sci. Technol.* **2015**, *5* (9), 4547−4555.
(31) Jenness, G. R.; Christiansen, M. A.; Caratzoulas, S.; Vlachos, D. G.; Gorte, R. J. Site-Dependent Lewis Acidity of gamma-Al2O3 and Its Impact on Ethanol Dehydration and Etherification. *J. Phys. Chem. C* **2014**, *118* (24), 12899−12907.
(32) Fang, Z. T.; Wang, Y.; Dixon, D. A. Computational Study of Ethanol Conversion on Al8O12 as a Model for gamma-Al_2O_3. *J. Phys. Chem. C* **2015**, *119* (41), 23413−23421.
(33) Dixit, M.; Kostetskyy, P.; Mpourmpakis, G. Structure Activity Relationships in Alkane Dehydrogenation on gamma-Al2O3: Site-Dependent Reactions. *ACS Catal.* **2018**, 11570.
(34) Pacchioni, G.; Bagas, P. S. CO Chemisorption on Oxide Surfaces: Bonding and Vibrations. *Cluster Models for Surface and Bulk Phenomena NATO ASI Ser., Ser. B* **1992**, *283*, 305.
(35) Becke, A. D. DENSITY-FUNCTIONAL THERMOCHEMISTRY.3. THE ROLE OF EXACT EXCHANGE. *J. Chem. Phys.* **1993**, *98* (7), 5648−5652.
(36) Lee, C. T.; Yang, W. T.; Parr, R. G. DEVELOPMENT OF THE COLLE-SALVETTI CORRELATION-ENERGY FORMULA INTO A FUNCTIONAL OF THE ELECTRON-DENSITY. *Phys. Rev. B: Condens. Matter Mater. Phys.* **1988**, *37* (2), 785−789.
(37) Frisch, M. J.; Schlegel, H. B.; Scuseria, G. E.; Robb, M. A.; Cheeseman, J. R.; Scalmani, G.; Barone, V.; Mennucci, B.; Petersson, G. A.; Nakatsuji, H.; Caricato, M.; Li, X.; Hratchian, H. P.; Izmaylov, A. F.; Bloino, J.; Zheng, G.; Sonnenberg, J. L.; Hada, M.; Ehara, M.; Toyota, K.; Fukuda, R.; Hasegawa, J.; Ishida, M.; Nakajima, T.; Honda, Y.; Kitao, O.; Nakai, H.; Vreven, T.; Montgomery, J. A., Jr.; Peralta, J. E.; Ogliaro, F.; Bearpark, M.; Heyd, J. J.; Brothers, E.; Kudin, K. N.; Staroverov, V. N.; Keith, T.; Kobayashi, R.; Normand, J.; Raghavachari, K.; Rendell, A.; Burant, J. C.; Iyengar, S. S.; Tomasi, J.; Cossi, M.; Rega, N.; Millam, J. M.; Klene, M.; Knox, J. E.; Cross, J. B.; Bakken, V.; Adamo, C.; Jaramillo, J.; Gomperts, R.; Stratmann, R. E.; Yazyev, O.; Austin, A. J.; Cammi, R.; Pomelli, C.; Ochterski, J. W.; Martin, R. L.; Morokuma, K.; Zakrzewski, V. G.; Voth, G. A.; Salvador, P.; Dannenberg, J. J.; Dapprich, S.; Daniels, A. D.; Farkas, O.; Foresman, J. B.; Ortiz, J. V.; Cioslowski, J.; Fox, D. J. *Gaussian 09*; Gaussian, Inc.: Wallingford, CT, 2010.
(38) Fukui, K. THE PATH OF CHEMICAL-REACTIONS - THE IRC APPROACH. *Acc. Chem. Res.* **1981**, *14* (12), 363−368.
(39) Kozuch, S.; Shaik, S. How to Conceptualize Catalytic Cycles? The Energetic Span Model. *Acc. Chem. Res.* **2011**, *44* (2), 101−110.
(40) Kostestkyy, P.; Maheswari, J. P.; Mpourmpakis, G. Understanding the Importance of Carbenium Ions in the Conversion of Biomass-Derived Alcohols with First-Principles Calculations. *J. Phys. Chem. C* **2015**, *119* (28), 16139−16147.

DOI: 10.1021/acs.iecr.8b04392
Ind. Eng. Chem. Res. 2018, 57, 16657−16663